Phase Tolerance Analysis in Planar Phased Arrays Through Minkowski Interval Analysis

L. Tenuti, N. Anselmi, P. Rocca, M. Salucci, and A. Massa

Abstract

Planar phased arrays are unavoidably affected by tolerances due to manufacturing errors, mutual coupling effects, mechanical deformations, and climatic changes. Assessing the impact of such non-idealities on the radiated pattern in clearly of fundamental importance, especially for critical applications such as monitoring, surveillance, and control. Towards this end, an innovative sensitivity tool has been developed to analyze the impact of phase tolerances in planar phased arrays on the radiation features. The proposed approach exploits the theory of interval analysis (*IA*), and makes use of the Minkowski sum to produce narrower bounds than classical Cartesian-*IA*. Some numerical results are shown, in order to prove the effectiveness of the developed Minkowski-*IA* approach, as well as to compare the generated pattern bounds with those determined through Cartesian-*IA*.

1 Numerical Assessment - Analysis vs Phase Tolerance

GOAL: this section considers the analysis of tolerances on the phase shifter of the control points of planar array with different number of elements, i.e., a 10×5 and a 10×10 planar array. The objective is to prove that, when tolerances on phase shifters are present the use of Minkowski intervals leads to sharpest bounds with respect to the use of Cartesian intervals. Moreover, it is necessary to investigate in which angular region (u, v) the Minkowski sum performs better bounds in comparison with the Cartesian sum.

Array geometry:

- Uniform planar array: $N \times M = 10 \times 5$, $N \times M = 10 \times 10$;
- Inter-element spacing: $d_x = 0.5$ $[\lambda]$ - $d_y = 0.5$ $[\lambda]$;

Nominal control points:

- Separable distributions:
  - x-axis: Dolph-Chebyshev pattern: $SLL = 20$ $[dB]$.
  - y-axis: Dolph-Chebyshev pattern: $SLL = 20$ $[dB]$.

Tolerances on the control points:

- Amplitude tolerance: $\delta\alpha_n = 0\,\%$.
- Phase tolerance: $\delta\beta_n = \pm 1$ $[deg]$, ± 3 $[deg]$, ± 5 $[deg]$.

Minkowski sum parameters:

- Number of sides including polygon: $L = 720$

1.1 10×5 Array Elements

Nominal Pattern

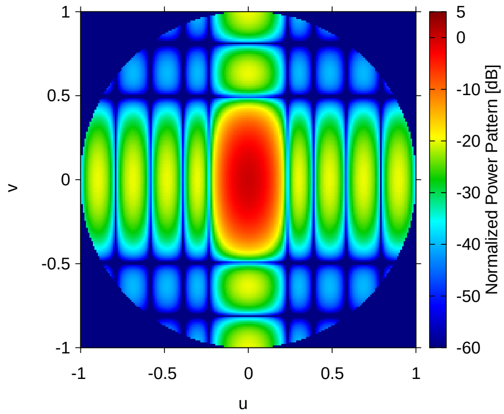

Figure 47:

Nominal Pattern Features

BW $[v] - u = 0$	BW $[u] - v = 0$	SLL $[dB] - u = 0$	SLL $[dB] - v = 0$	PP $[dB]$
0.412	0.196	-20.0	-20.0	29.29

Table XV:

1.1.1 Phase Error ± 1 $[deg]$

Interval Pattern

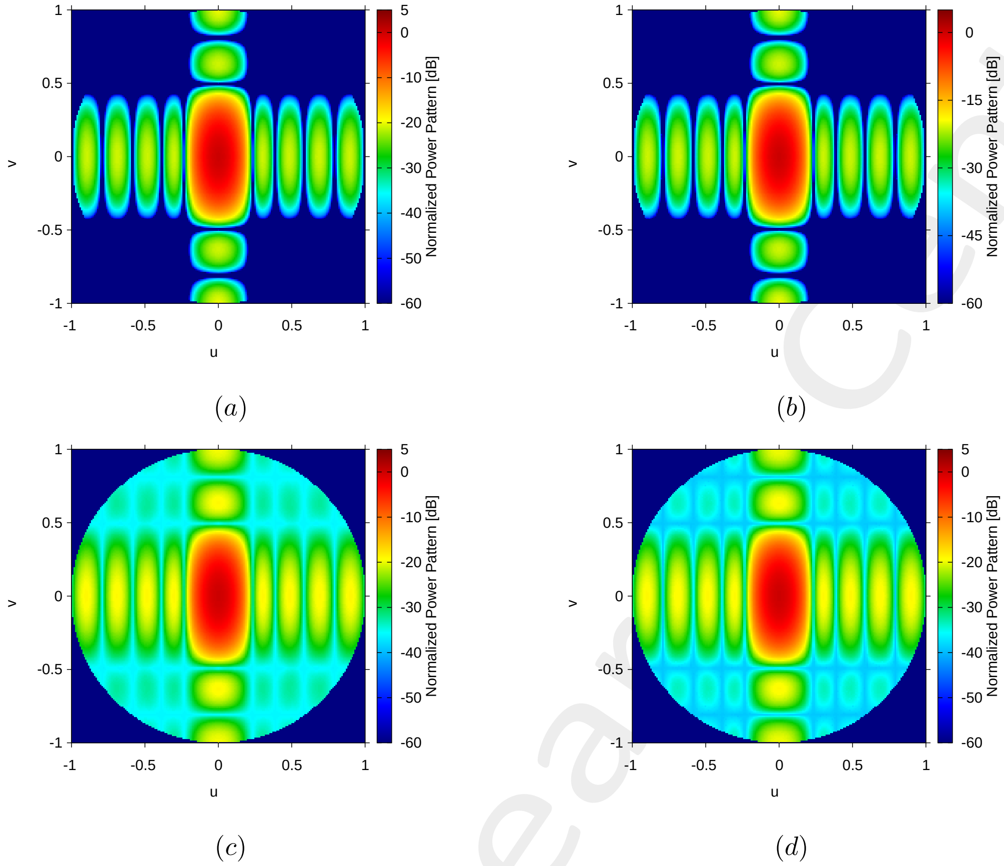

Figure 48: Infimum of the power pattern Cartesian (a) and Minkowski sum (b), Supremum of the sum power pattern Cartesian (c) and Minkowski (d) sum

Cuts on the plane $(0, v)$ - $(u, 0)$ - Interval Pattern

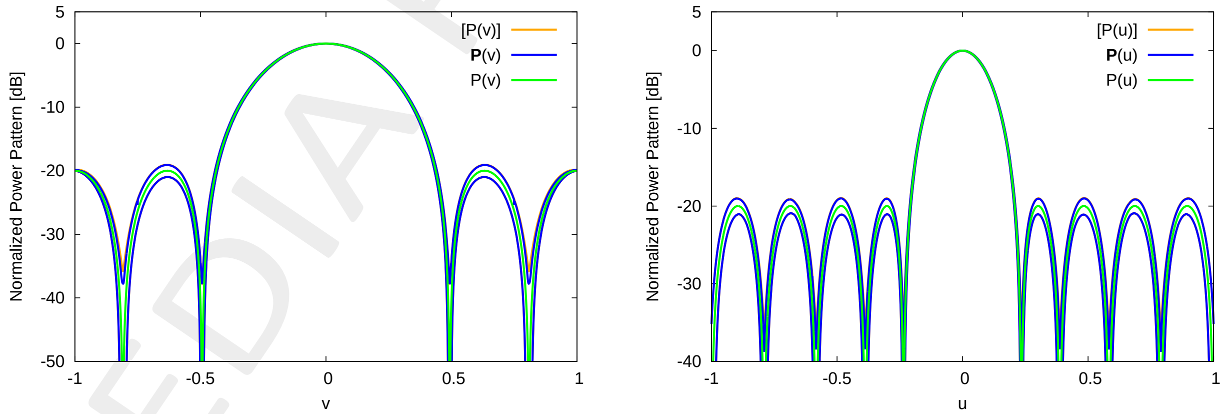

(a) (b)

Figure 49:

Cuts on the plane $(0.300, v)$ **-** $(u, 0.632)$ **- Interval Pattern**

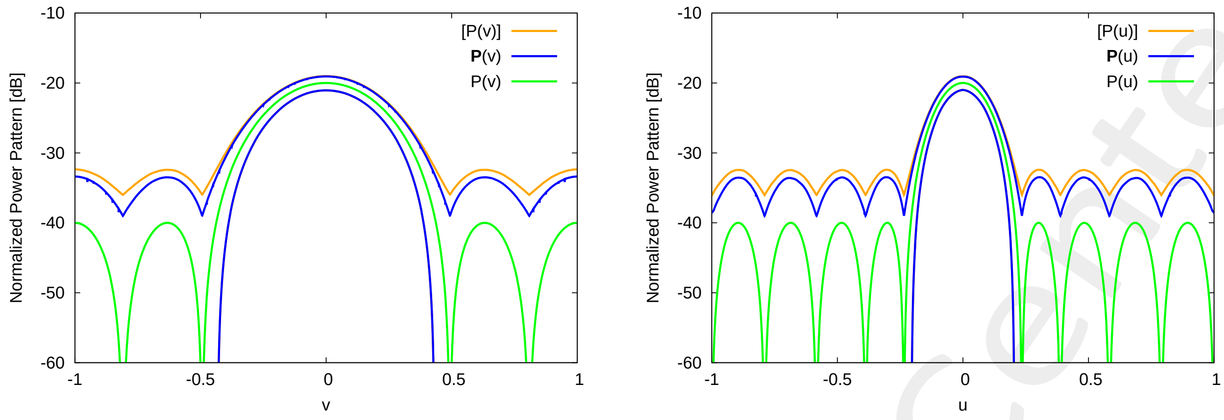

(a) (b)

Figure 50:

1.1.2 Phase Error ± 3 $[deg]$

Interval Pattern

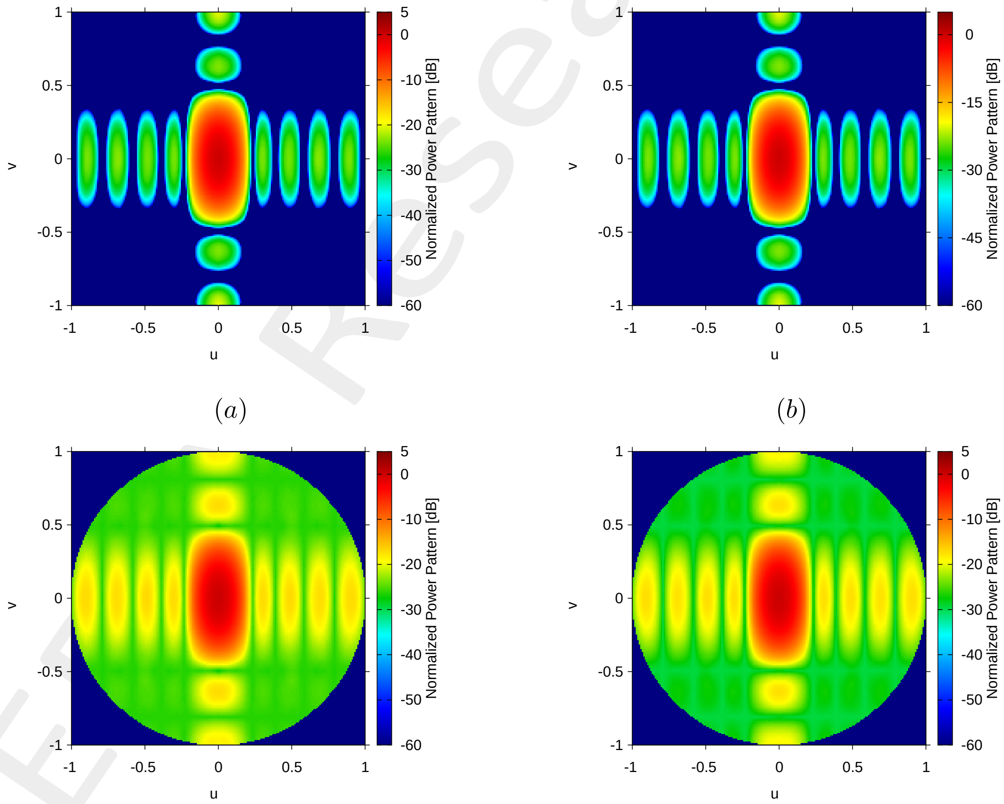

(a) (b)

(c) (d)

Figure 51: Infimum of the power pattern Cartesian (a) and Minkowski sum (b), Supremum of the sum power pattern Cartesian (c) and Minkowski (d) sum

Cuts on the plane $(0, v)$ **-** $(u, 0)$ **- Interval Pattern**

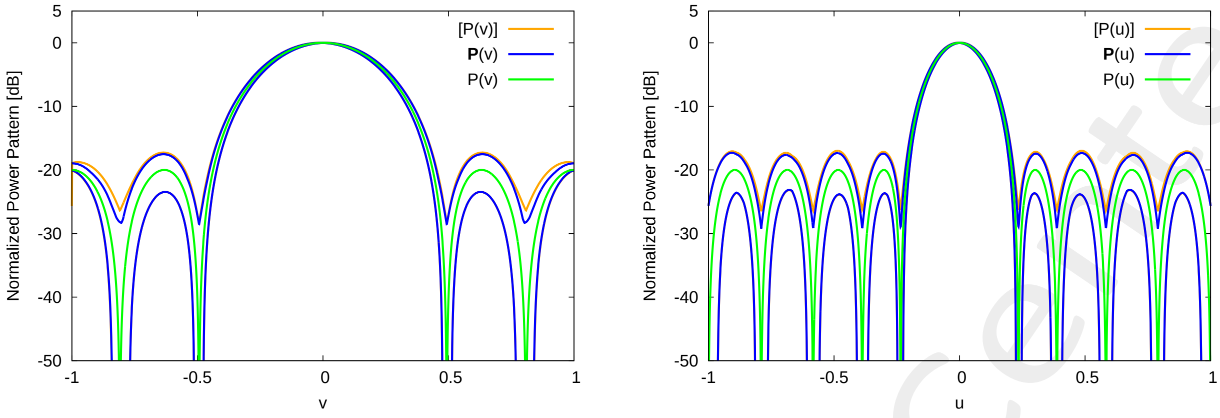

(a) (b)

Figure 52:

Cuts on the plane $(0.300, v)$ **-** $(u, 0.632)$ **- Interval Pattern**

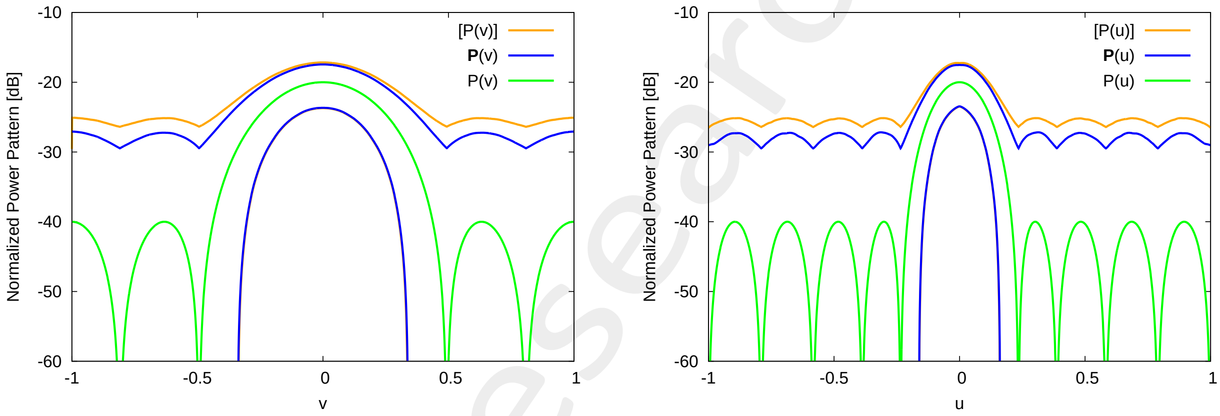

(a) (b)

Figure 53:

1.1.3 Phase Error ± 5 $[deg]$

Interval Pattern

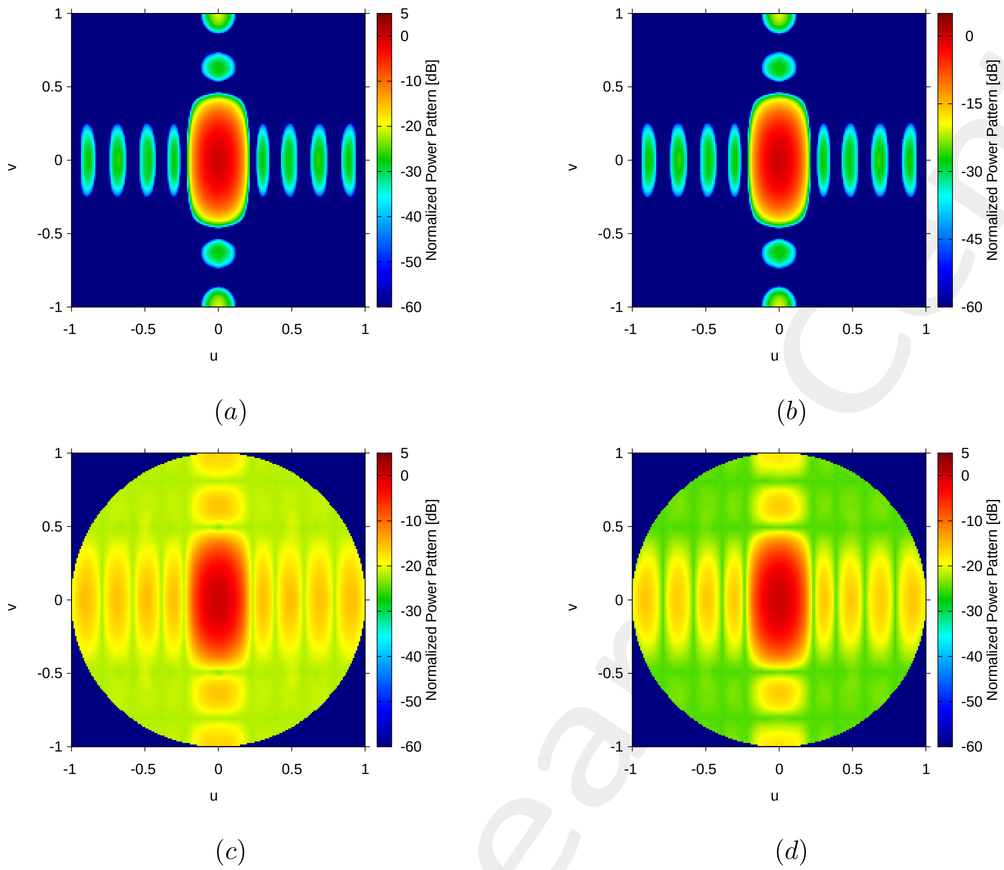

Figure 54: Infimum of the power pattern Cartesian (a) and Minkowski sum (b), Supremum of the sum power pattern Cartesian (c) and Minkowski (d) sum

Cuts on the plane $(0, v)$ - $(u, 0)$ - Interval Pattern

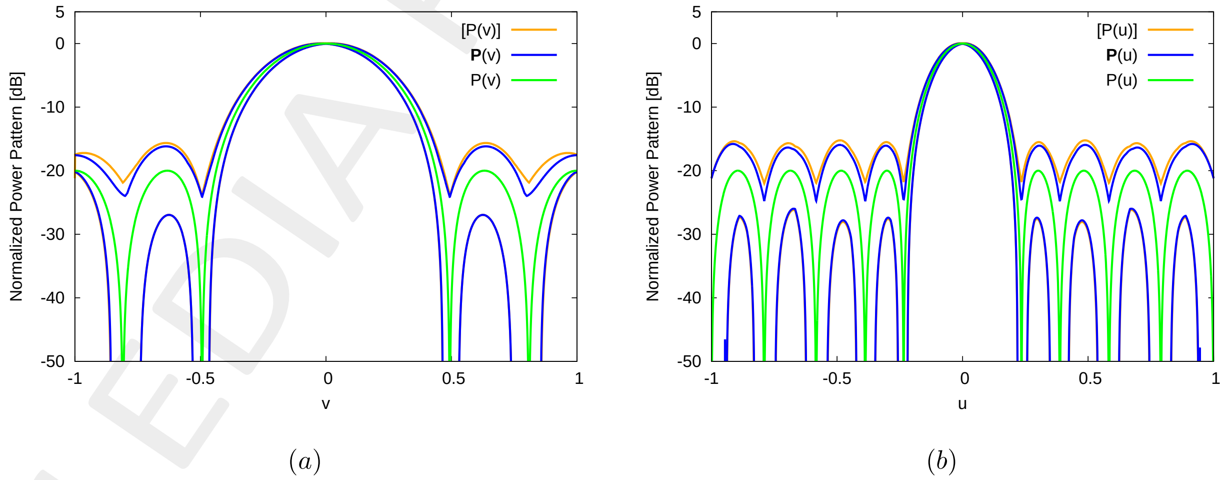

Figure 55:

Cuts on the plane $(0.300, v)$ - $(u, 0.632)$ - Interval Pattern

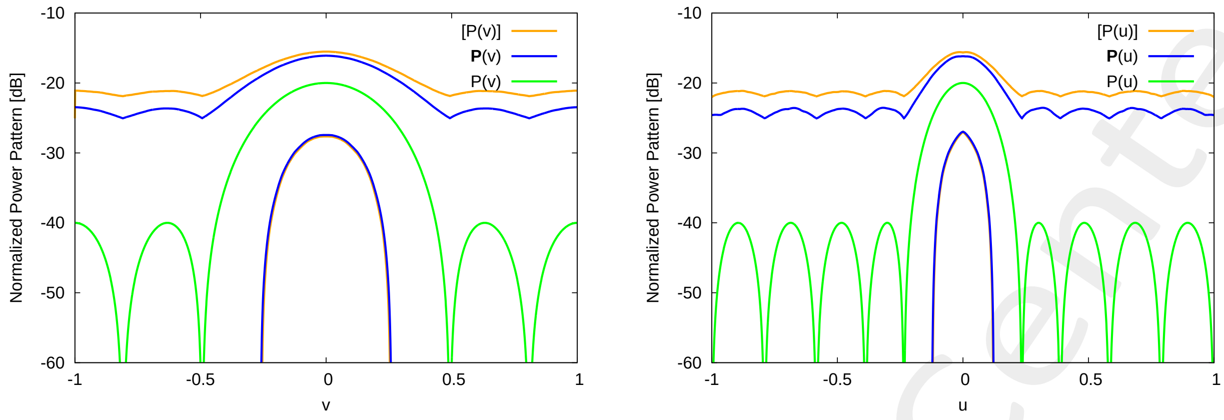

(a) (b)

Figure 56:

1.1.4 Analysis vs Phase Tolerance

Pattern: Cuts on the plane $(0, v)$ - $(u, 0)$

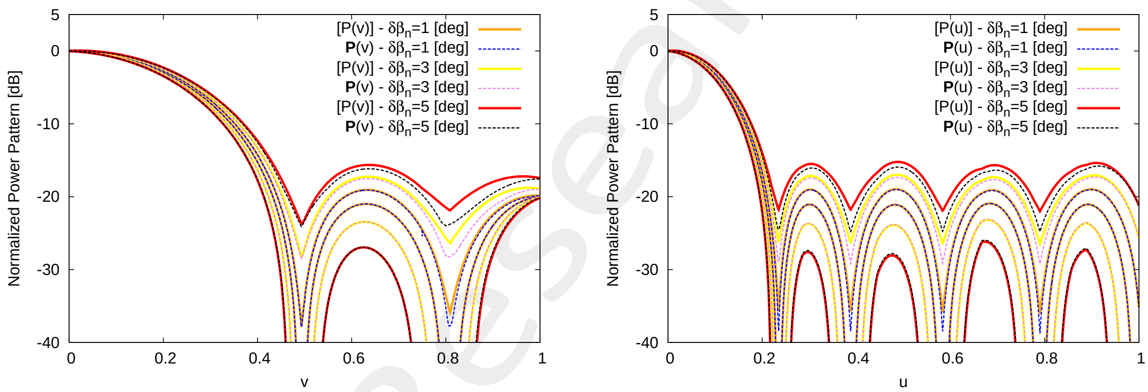

(a) (b)

Figure 57:

Pattern: Cuts on the plane $(0.300, v)$ - $(u, 0.632)$

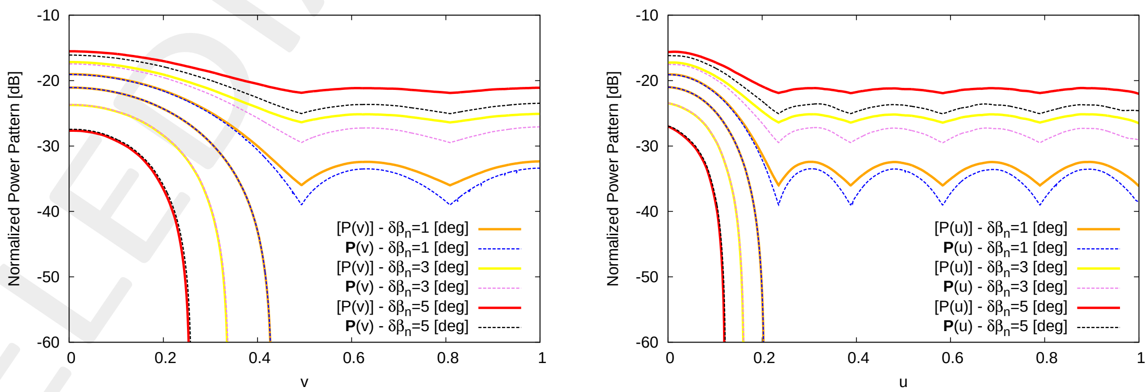

(a) (b)

Figure 58:

Interval Beamwidth

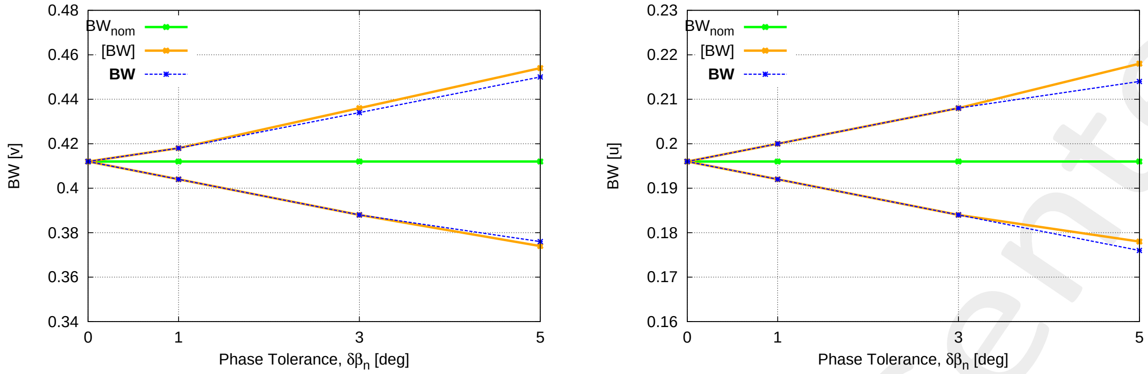

(a) (b)

Figure 59:

Interval SLL

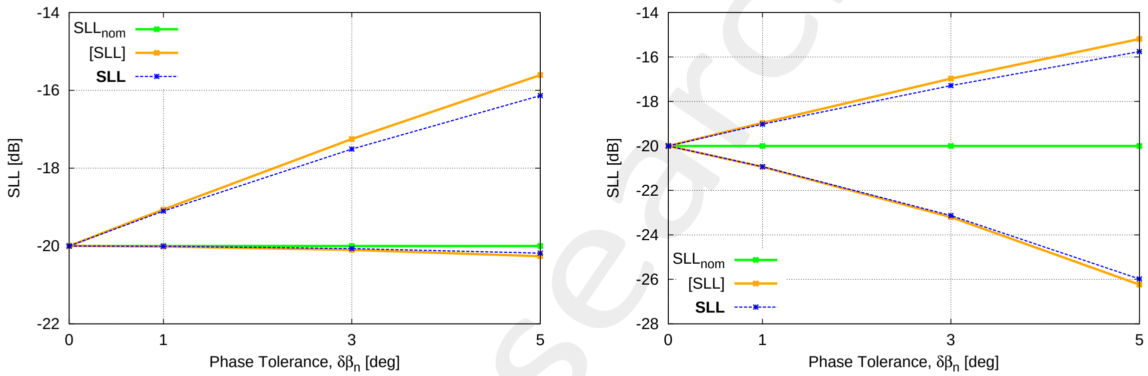

(a) (b)

Figure 60:

Interval Normalized Power Peak vs Amplitude Tolerance

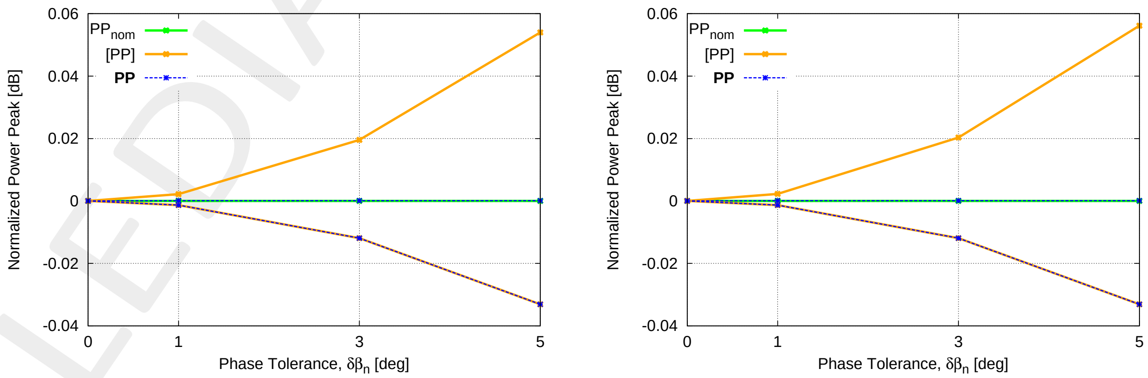

(a) (b)

Figure 61:

Pattern Matching and Normalized Pattern Matching

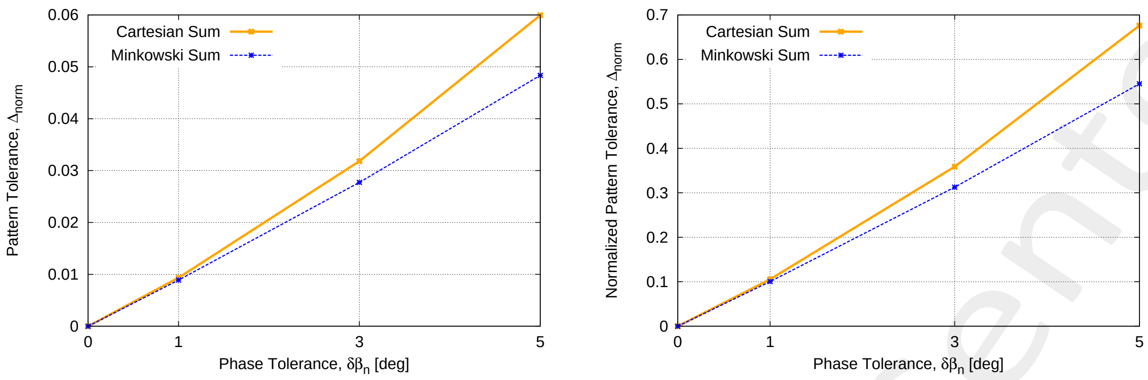

(a) (b)

Figure 62:

Interval Pattern Features - Cuts on the plane $(0, v)$ - $(u, 0)$

Plane $u = 0$

	Cartesian Sum			*Minkowski Sum*		
$\delta\beta_n$ [*deg*]	$[BW]$ [u]	SLL [dB]	$[PP]$ [dB]	$[BW]$ [u]	$[SLL]$ [dB]	PP [dB]
±1	$[0.404, 0.418]$	$[-20.01, -19.06]$	$[29.28, 29.29]$	$[0.404, 0.418]$	$[-20.00, -19.10]$	$[29.28, 29.29]$
±3	$[0.388, 0.436]$	$[-20.10, -17.25]$	$[29.27, 29.30]$	$[0.388, 0.434]$	$[-20.07, -17.51]$	$[29.27, 29.29]$
±5	$[0.374, 0.454]$	$[-20.26, -15.61]$	$[29.25, 29.34]$	$[0.376, 0.450]$	$[-20.18, -16.14]$	$[29.25, 29.29]$

Table XVI:

Plane $v = 0$

	Cartesian Sum			*Minkowski Sum*		
$\delta\beta_n$ [*deg*]	$[BW]$ [u]	SLL [dB]	$[PP]$ [dB]	$[BW]$ [u]	$[SLL]$ [dB]	PP [dB]
±1	$[0.192, 0.200]$	$[-20.94, -18.96]$	$[29.28, 29.29]$	$[0.192, 0.200]$	$[-20.93, -19.02]$	$[29.28, 29.29]$
±3	$[0.184, 0.208]$	$[-23.20, -16.97]$	$[29.27, 29.30]$	$[0.184, 0.208]$	$[-23.13, -17.29]$	$[29.27, 29.29]$
±5	$[0.178, 0.218]$	$[-26.23, -15.19]$	$[29.25, 29.34]$	$[0.176, 0.214]$	$[-25.98, -15.76]$	$[29.25, 29.29]$

Table $XVII$:

Pattern Matching Δ- Δ_{norm}

	Cartesian Sum		*Minkowski Sum*	
$\delta\beta_n$ [*deg*]	Δ	Δ_{norm}	Δ	Δ_{norm}
±1	9.35×10^{-3}	0.105	8.89×10^{-3}	0.100
±3	3.18×10^{-2}	0.359	2.77×10^{-2}	0.312

± 5	5.99×10^{-2}	0.676	4.83×10^{-2}	0.545

Table $XVIII$:

1.1.5 Comments and Observations:

The utilization of the Minkowski sum leads to sharpest bounds of the interval power pattern with respect to the Cartesian sum. Such a result is evident expecially in the side lobe region far from the the planes $u = 0$ and $v = 0$. This can be explained considering that for those planes the cartesian inclusion is very close to the Minkowski inclusion (as seen for $u = 0$ in linear arrays). The results are the same for all the values of tolerances on the phase shifters. This is graphical confirmed by the bounds on the pattern and by the interval parameters as well as the values of Δ and Δ_{norm}. As expected, increasing the value of the tolerance on the phase shifters from ± 1 $[deg]$ to ± 5 $[deg]$ the bounds increase.

1.2 10×10 Array Elements

Nominal Pattern

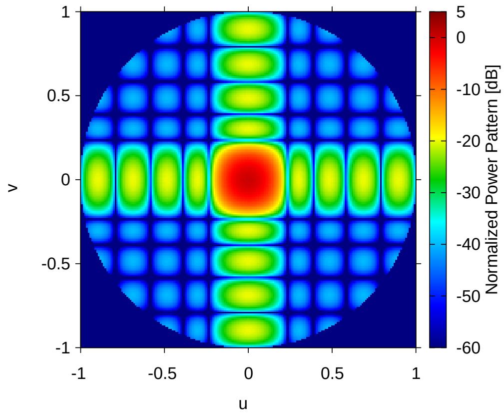

Figure 63:

Nominal Pattern Features

$BW\ [v] - u = 0$	$BW\ [u] - v = 0$	$SLL\ [dB] - u = 0$	$SLL\ [dB] - v = 0$	$PP\ [dB]$
0.196	0.196	-20.0	-20.0	35.84

Table XIX:

1.2.1 Phase Error ± 1 $[deg]$

Interval Pattern

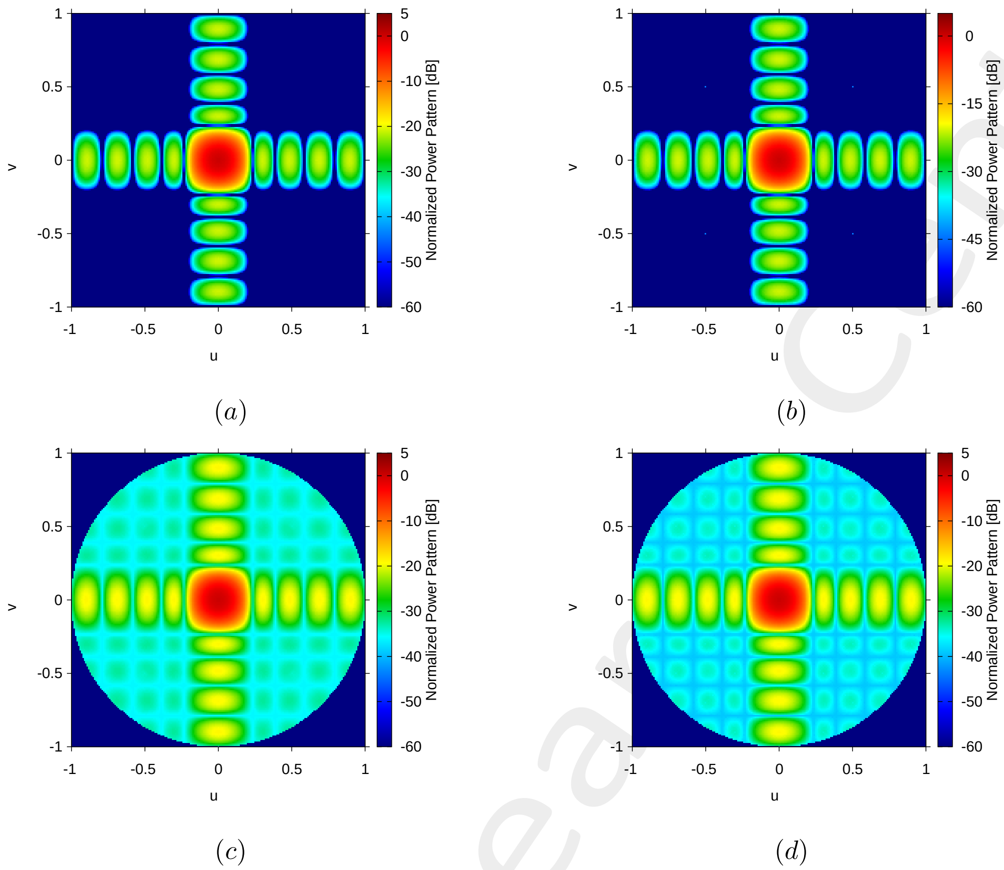

Figure 64: Infimum of the power pattern Cartesian (a) and Minkowski sum (b), Supremum of the sum power pattern Cartesian (c) and Minkowski (d) sum

Cuts on the plane $(0, v)$ - $(u, 0)$ - Interval Pattern

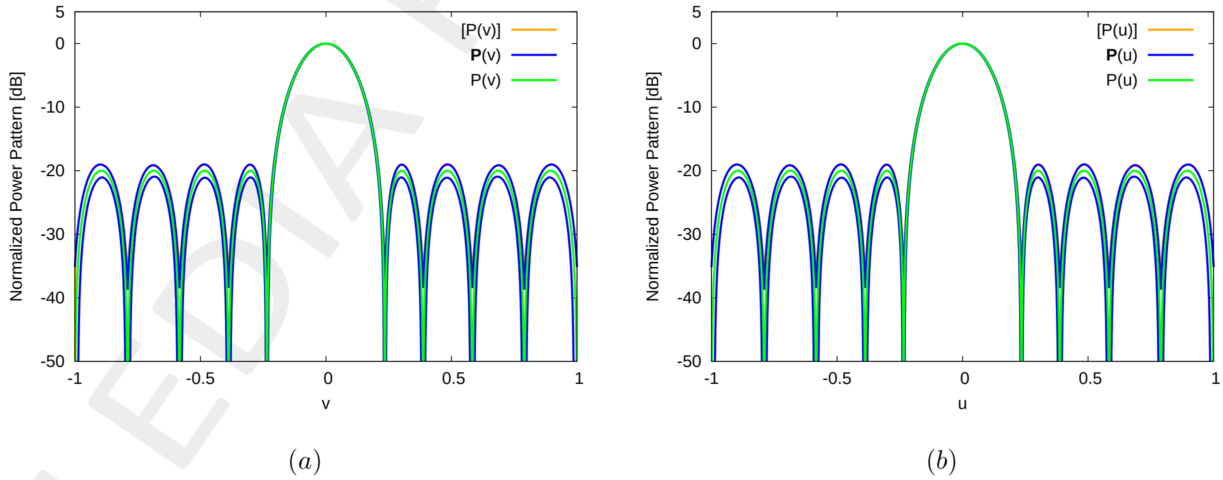

Figure 65:

Cuts on the plane $(0.300, v)$ - $(u, 0.632)$ - Interval Pattern

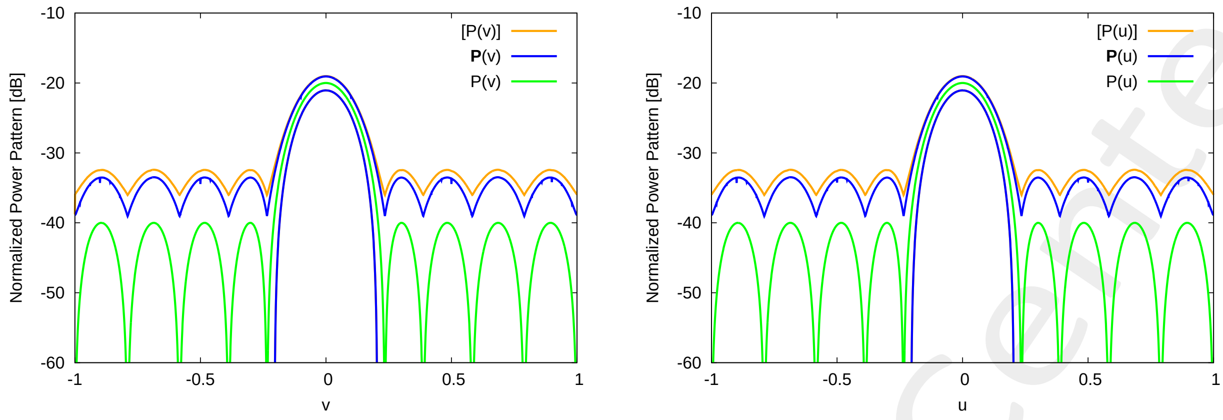

(a) (b)

Figure 66:

1.2.2 Phase Error ± 3 $[deg]$

Interval Pattern

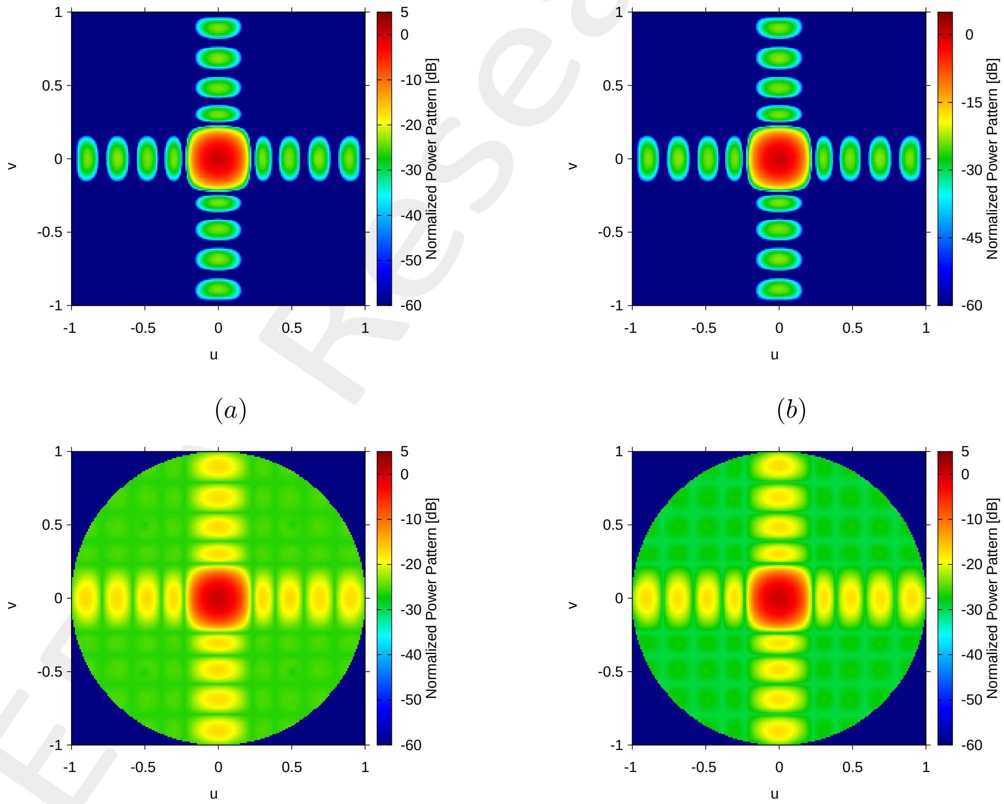

(a) (b)

(c) (d)

Figure 67: Infimum of the power pattern Cartesian (a) and Minkowski sum (b), Supremum of the sum power pattern Cartesian (c) and Minkowski (d) sum

Cuts on the plane $(0, v)$ - $(u, 0)$ - Interval Pattern

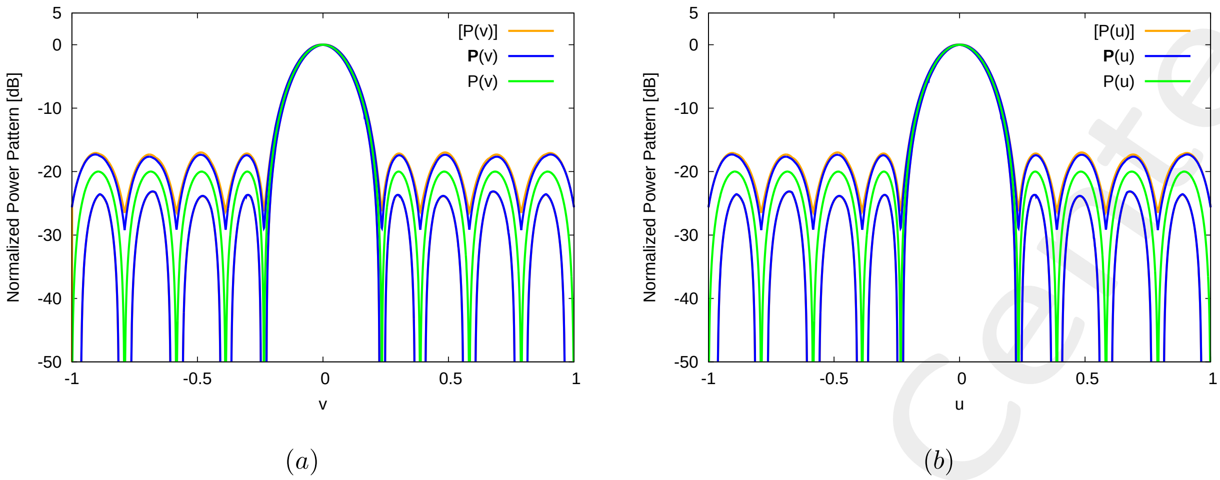

Figure 68:

Cuts on the plane $(0.300, v)$ - $(u, 0.632)$ - Interval Pattern

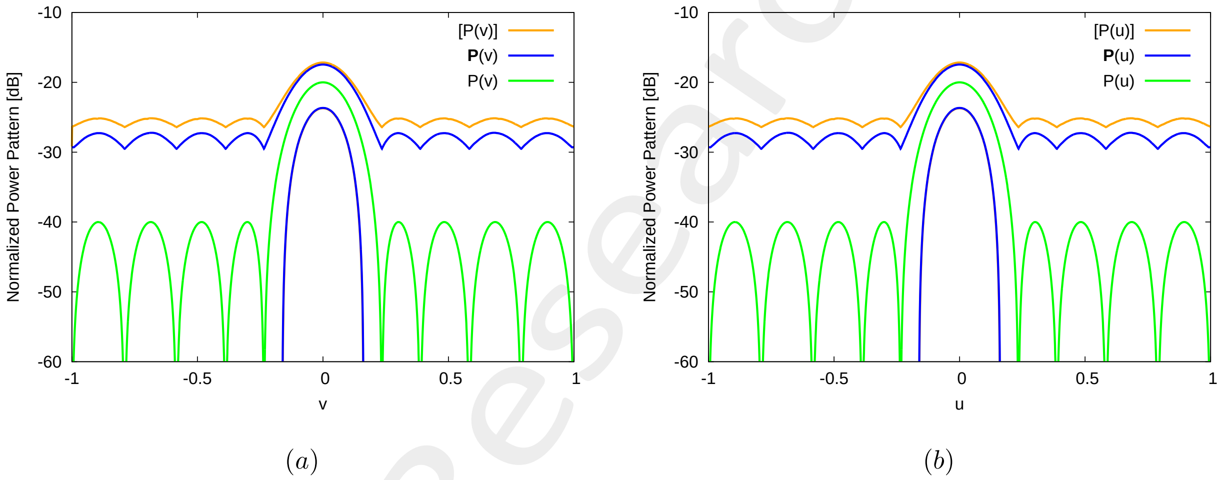

Figure 69:

1.2.3 Phase Error ± 5 $[deg]$

Interval Pattern

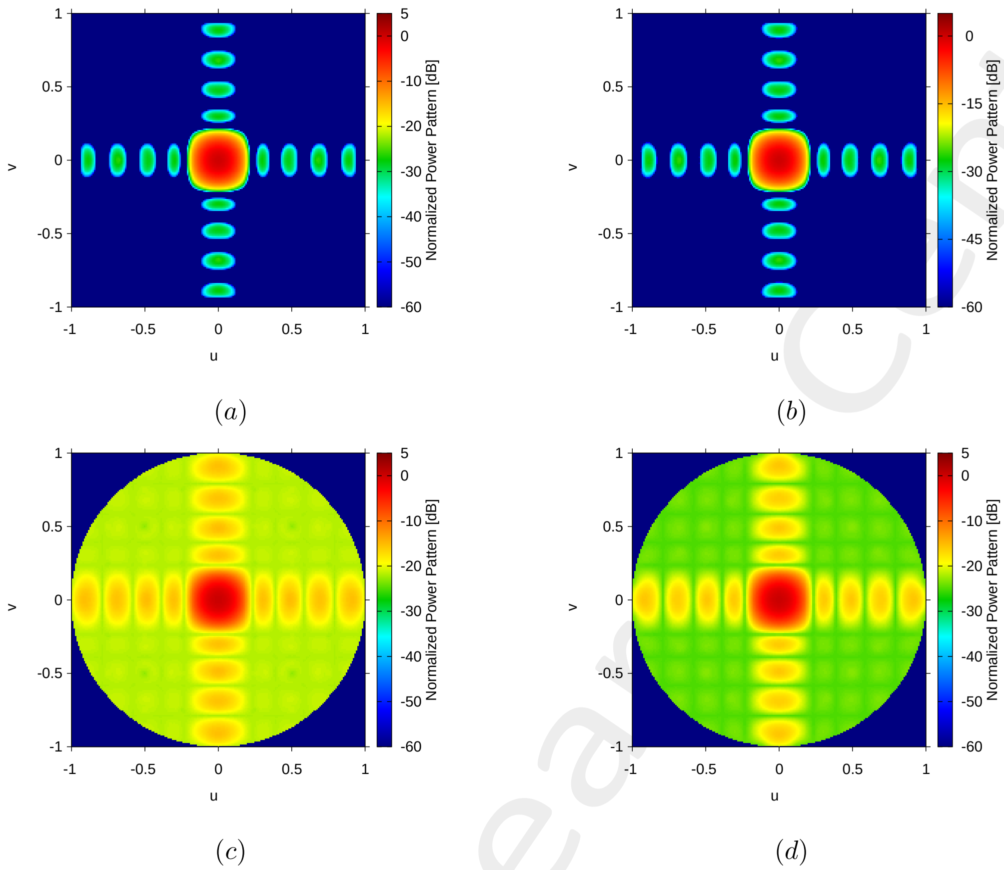

Figure 70: Infimum of the power pattern Cartesian (a) and Minkowski sum (b), Supremum of the sum power pattern Cartesian (c) and Minkowski (d) sum

Cuts on the plane $(0, v)$ - $(u, 0)$ - Interval Pattern

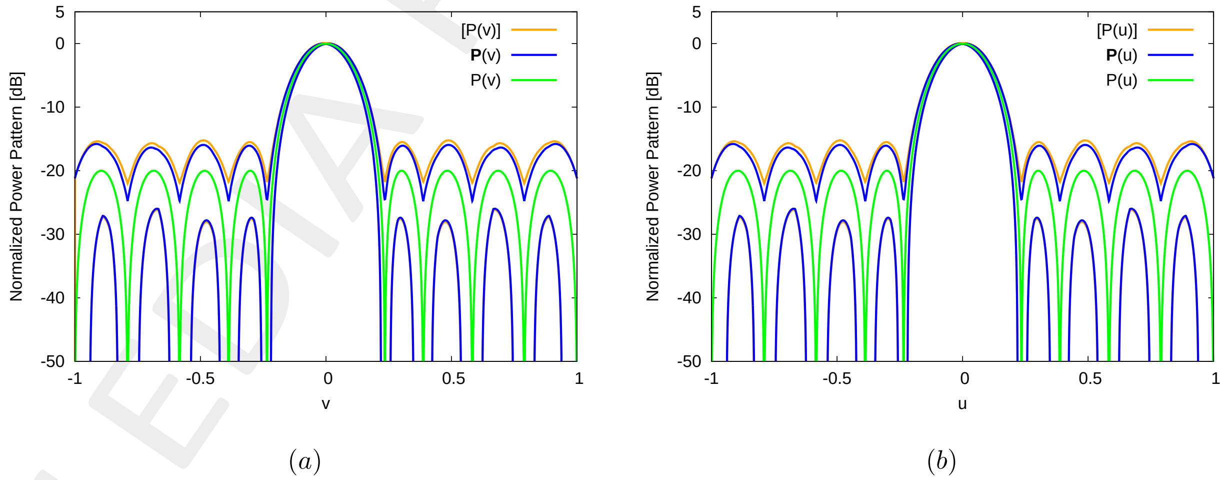

Figure 71:

Cuts on the plane $(0.300, v)$ **-** $(u, 0.632)$ **- Interval Pattern**

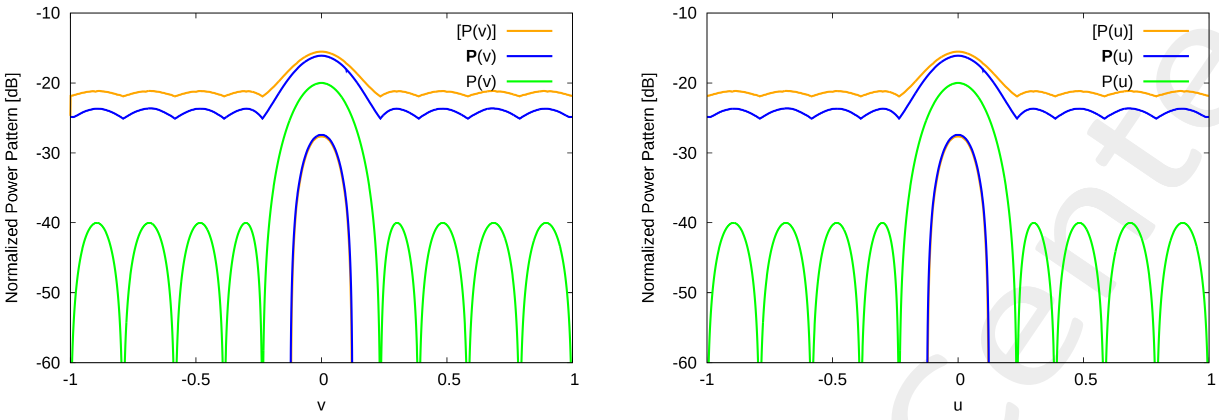

(a) (b)

Figure 72:

1.2.4 Analysis vs Phase Tolerance

Pattern: Cuts on the plane $(0, v)$ **-** $(u, 0)$

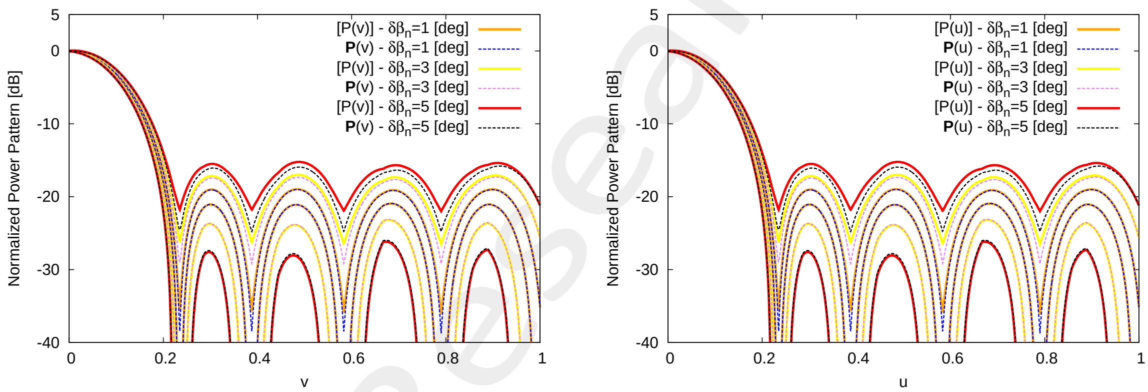

(a) (b)

Figure 73:

Pattern: Cuts on the plane $(0.300, v)$ **-** $(u, 0.632)$

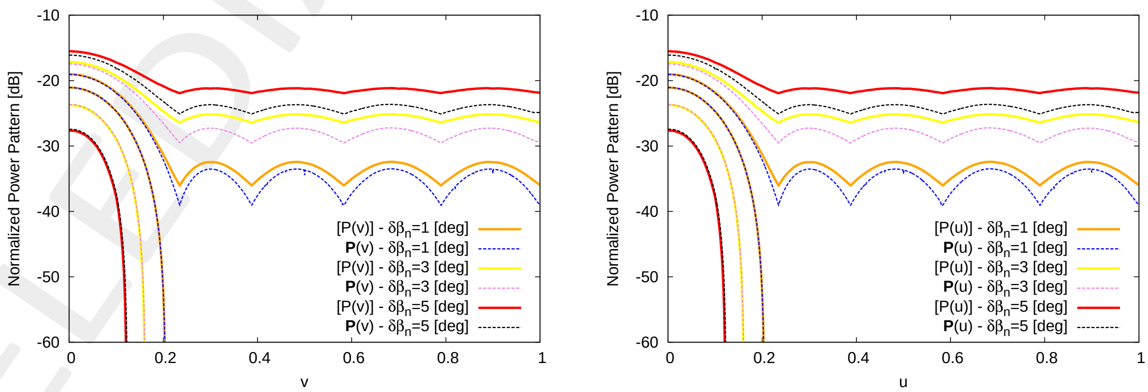

(a) (b)

Figure74:

Interval Beamwidth

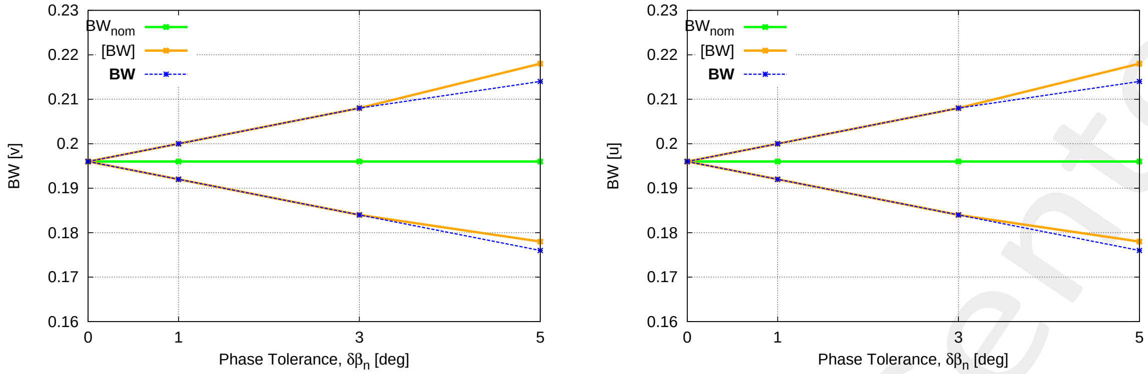

(a) (b)

Figure 75:

Interval SLL

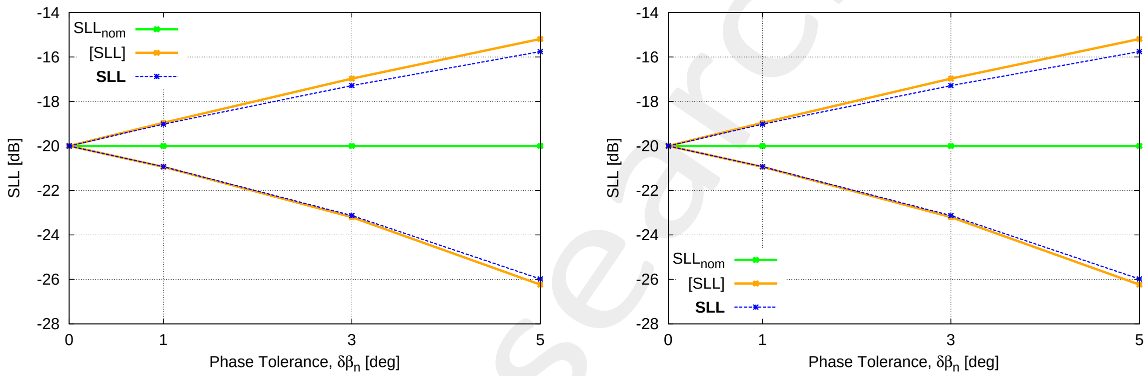

(a) (b)

Figure 76:

Interval Normalized Power Peak vs Amplitude Tolerance

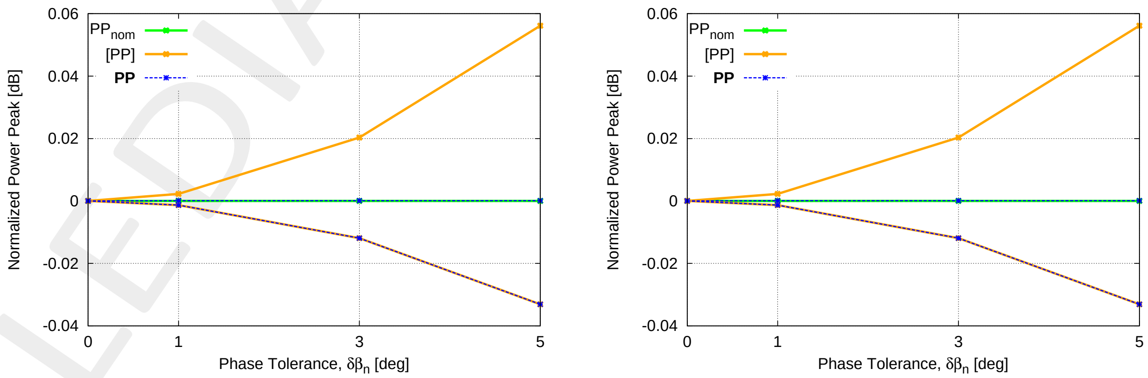

(a) (b)

Figure 77:

Pattern Matching and Normalized Pattern Matching

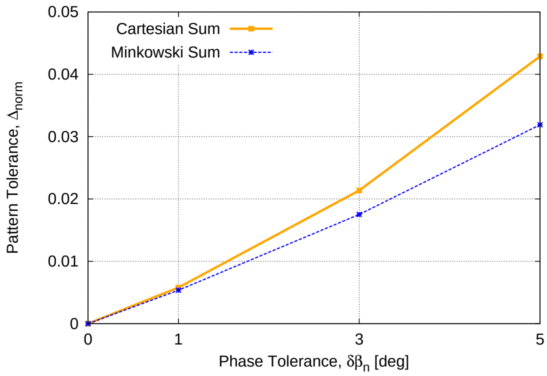

(a)

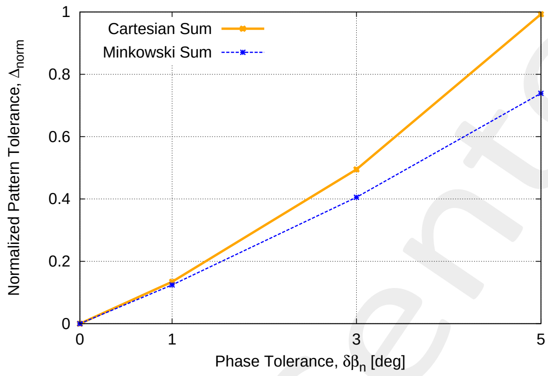

(b)

Figure 78:

Interval Pattern Features - Cuts on the plane $(0, v)$ - $(u, 0)$

Plane $u = 0$

	Cartesian Sum			*Minkowski Sum*		
$\delta\beta_n$ [*deg*]	[*BW*] [*u*]	*SLL* [*dB*]	[*PP*] [*dB*]	[*BW*] [*u*]	[*SLL*] [*dB*]	*PP* [*dB*]
± 1	[0.192, 0.200]	[−20.94, −18.96]	[35.84, 35.84]	[0.192, 0.200]	[−20.93, −19.02]	[35.84, 35.84]
± 3	[0.184, 0.208]	[−23.20, −16.97]	[35.83, 35.84]	[0.184, 0.208]	[−23.13, −17.29]	[35.83, 35.84]
± 5	[0.178, 0.218]	[−26.23, −15.19]	[35.81, 35.90]	[0.176, 0.214]	[−25.98, −15.76]	[35.81, 35.84]

Table *XX*:

Plane $v = 0$

	Cartesian Sum			*Minkowski Sum*		
$\delta\beta_n$ [*deg*]	[*BW*] [*u*]	*SLL* [*dB*]	[*PP*] [*dB*]	[*BW*] [*u*]	[*SLL*] [*dB*]	*PP* [*dB*]
± 1	[0.192, 0.200]	[−20.94, −18.96]	[35.84, 35.84]	[0.192, 0.200]	[−20.93, −19.02]	[35.84, 35.84]
± 3	[0.184, 0.208]	[−23.20, −16.97]	[35.83, 35.84]	[0.184, 0.208]	[−23.13, −17.29]	[35.83, 35.84]
± 5	[0.178, 0.218]	[−26.23, −15.19]	[35.81, 35.90]	[0.176, 0.214]	[−25.98, −15.76]	[35.81, 35.84]

Table *XXI*:

Pattern Matching Δ- Δ_{norm}

	Cartesian Sum		*Minkowski Sum*	
$\delta\beta_n$ [*deg*]	Δ	Δ_{norm}	Δ	Δ_{norm}
± 1	5.80×10^{-3}	0.134	5.37×10^{-3}	0.124
± 3	2.14×10^{-2}	0.495	1.75×10^{-2}	0.405
± 5	4.29×10^{-2}	0.993	3.19×10^{-2}	0.739

Table $XXII$:

1.2.5 Comments and Observations:

The utilization of the Minkowski sum leads to sharpest bounds of the interval power pattern with respect to the Cartesian sum. Such a result is evident expecially in the side lobe region far from the the planes $u = 0$ and $v = 0$. This can be explained considering that for those planes the cartesian inclusion is very close to the Minkowski inclusion (as seen for $u = 0$ in linear arrays). The results are the same for all the values of tolerances on the phase shifters. This is graphical confirmed by the bounds on the pattern and by the interval parameters as well as the values of Δ and Δ_{norm}. As expected, increasing the value of the tolerance on the phase shifters from ±1 $[deg]$ to ±5 $[deg]$ the bounds increase.

References

[1] N. Anselmi, P. Rocca, M. Salucci, and A. Massa, "Optimization of excitation tolerances for robust beamforming in linear arrays," *IET Microw. Antennas Propag.*, vol. 10, no. 2, pp. 208-214, 2016.

[2] P. Rocca, G. Oliveri, R. J. Mailloux, and A. Massa, "Unconventional phased array architectures and design Methodologies - A review," *Proc. IEEE*, vol. 104, no. 3, pp. 544-560, Mar. 2016.

[3] G. Oliveri, M. Salucci, and A. Massa, "Synthesis of modular contiguously clustered linear arrays through a sparseness-regularized solver," *IEEE Trans. Antennas Propag,*, vol. 64, no. 10, pp. 4277-4287, Oct. 2016.

[4] L. Poli, P. Rocca, N. Anselmi, and A. Massa, "Dealing with uncertainties on phase weighting of linear antenna arrays by means of interval-based tolerance analysis," *IEEE Trans. Antennas Propag.*, vol. 63, no. 7, pp. 3299-3234, Jul. 2015.

[5] P. Rocca, N. Anselmi, and A. Massa, "Optimal synthesis of robust beamformer weights exploiting interval analysis and convex optimization," *IEEE Trans. Antennas Propag.*, vol. 62, no. 7, pp. 3603-3612, Jul. 2014.

[6] L. Manica, N. Anselmi, P. Rocca, and A. Massa, "Robust mask-constrained linear array synthesis through an interval-based particle swarm optimisation," *IET Microw. Antennas Propag.*, vol. 7, no. 12, pp. 976-984, Sep. 2013.

[7] N. Anselmi, L. Manica, P. Rocca, and A. Massa, "Tolerance analysis of antenna arrays through interval arithmetic," *IEEE Trans. Antennas Propag.*, vol. 61, no. 11, pp. 5496-5507, Nov. 2013.

[8] P. Rocca, L. Manica, N. Anselmi, and A. Massa, "Analysis of the pattern tolerances in linear arrays with arbitrary amplitude errors," *IEEE Antennas Wireless Propag. Lett.*, vol. 12, pp. 639-642, 2013.

[9] T. Moriyama, L. Poli, N. Anselmi, M. Salucci, and P. Rocca, "Real array pattern tolerances from amplitude excitation errors," *IEICE Electron. Express*, vol. 11, no. 17, pp. 1-8, Sep. 2014.

[10] P. Rocca, N. Anselmi, and A. Massa, "Optimal synthesis of robust array configurations exploiting interval analysis and convex optimization," *IEEE Trans. Antennas Propag.*, vol. 62, no. 7, pp. 3603-3612, Jul. 2014.

[11] N. Anselmi, P. Rocca, M. Salucci, and A. Massa, "Power pattern sensitivity to calibration errors and mutual coupling in linear arrays through circular interval arithmetics," *Sensors*, vol. 16, no. 6 (791), pp. 1-14, 2016.

[12] L. Tenuti, N. Anselmi, P. Rocca, M. Salucci, and A. Massa, "Minkowski sum method for planar arrays sensitivity analysis with uncertain-but-bounded excitation tolerances," *IEEE Trans. Antennas Propag.*, vol. 65, no. 1, pp. 167-177, Jan. 2017.

[13] P. Rocca, N. Anselmi, and A. Massa, "Interval Arithmetic for pattern tolerance analysis of parabolic reflectors," *IEEE Trans. Antennas Propag.*, vol. 62, no. 10, pp. 4952-4960, Oct. 2014.

[14] P. Rocca, L. Poli, N. Anselmi, M. Salucci, and A. Massa, "Predicting antenna pattern degradations in microstrip reflectarrays through interval arithmetic," *IET Microw. Antennas Propag.*, vol. 10, no. 8, pp. 817-826, May 2016.

[15] N. Anselmi, M. Salucci, P. Rocca, and A. Massa, "Generalized sensitivity analysis tool for pattern distortions in reflector antennas with bump-like surface deformations," *IET Microw. Antennas Propag.*, vol. 10, no. 9, p. 909-916, Jun. 2016.